van der Waals–London dispersion interactions for optically anisotropic cylinders: Metallic and semiconducting single-wall carbon nanotubes

Rick F. Rajter,[1] Rudi Podgornik,[2,3] V. Adrian Parsegian,[2] Roger H. French,[4] and W. Y. Ching[5]

[1]*Department of Materials Science and Engineering, MIT, Cambridge, Massachusetts 02139-4307, USA*

[2]*Laboratory of Physical and Structural Biology, NICHD, National Institutes of Health, Bethesda, Maryland 20892-0924, USA*

[3]*Faculty of Mathematics and Physics, University of Ljubljana, Ljubljana SI-1000, Slovenia and Department of Theoretical Physics, J. Stefan Institute, Ljubljana 1000, Slovenia*

[4]*DuPont Co. Central Research, Experimental Station, E400-5207, Wilmington, Delaware 19880, USA*

[5]*Department of Physics, University of Missouri–Kansas City, Kansas City, Missouri 64110, USA*

We investigate the van der Waals–London dispersion interactions between a single-walled carbon nanotube immersed in water and interacting with three different objects: an optically isotropic planar substrate, an optically anisotropic planar substrate, and another single-walled carbon nanotube of identical chirality. These interactions were derived from *ab initio* optical properties and an appropriate formulation of the Lifshitz theory. We derive two analytically tractable limits for the van der Waals interaction: the far limit at separations much larger than the cylinder radius, and the near or Derjaguin limit where surface-cylinder separation is much smaller than the radius. We investigate in detail the effect of relative geometry and the relative separation on the magnitude of the dispersion interaction.

I. INTRODUCTION

Single-wall carbon nanotubes (SWCNTs) have received an extraordinary amount of attention since their discovery in 1991.[1,2] One unique feature of this class of materials is how much their electronic properties can change with respect to subtle changes in the wrapping angle, or chirality, of each particular carbon nanotube (CNT).[3,4] Many researchers classify SWCNTs into two broad categories: metallic and semiconducting.[5] The metallic tubes have a chirality such that $[(n-m)\text{Mod }3=0]$, where n and m are the lattice translation vectors for a simple sheet of graphene. All other combinations of n and m yield SWCNTs with a band gap and are thus semiconducting. The origin and reasoning behind the electronic structure's dependence on chirality are well documented from both band-structure theory and experimental results, and are based heavily on the continuous nature of the graphene band structure becoming discretized because of the imposed finite distance in the circumferential direction. The metallic tubes are the SWCNTs that have these allowable states cross the k points of graphene.[6]

The literature often ignores the full frequency-dependent dielectric spectrum of the SWCNTs. This is largely due to two major reasons: First, people interested in electronic conduction focus particularly on the band gap. Second, it is nontrivial to measure accurately full spectral data. While it is true that these data are not necessarily important for the performance of a particular device, they are critical for making devices that involve the placement and/or arrangement of SWCNTs. Fortunately, computational power and efficient, robust quantum-mechanical codes have been developed to give us the very accurate spectral data needed for analyzing these interactions.[7–11] Additionally, it has been discovered that the dielectric spectral data nonlinearly depend on chirality and some SWCNTs even exhibit significant optical anisotropy between their radial and axial directions.[12,13] For the

purposes of this paper, one CNT was selected out of each of the two major SWCNT classes (the $[6,5,s]$ semiconducting and $[9,3,m]$ metallic, which have been previously analyzed[13]). This is not to suggest that all or even any tubes in each category will behave alike. In fact, it is possible to group SWCNTs into three different classes (metals, semimetals [very small gap semiconductors], and semiconductors), by families,[14] or have no classification system at all. While the taxonomy and correlation of van der Waals–London dispersion (vdW-Ld) spectra to chirality is very interesting in itself, it is not the focus of this paper and will be analyzed in the future. Rather, the focus is on the methodology of going from each SWCNT's van der Waals–London dispersion spectrum to calculate the van der Waals–London dispersion interaction energy that results from the SWCNT's shape and optical anisotropy.

The van der Waals–London dispersion interactions dominate systems that have no net charge and in which typical separations are much larger than those characteristic of molecular and atomic bonds. They are particularly important in colloidal systems and, in fact, determine the colloidal stability as formalized within the standard Derjaguin-Landau-Verwey-Overbeek theory.[15] A proper understanding and a consistent theoretical formulation of the van der Waals–London dispersion interaction have been fully achieved within the Lifshitz theory of dispersion interactions.[16,17] It provides the link between dielectric dispersion spectra and the magnitude of these interactions for geometries that are either analytically tractable or easily approximated into simpler geometries. For systems with anisotropic dielectric response, such as SWCNTs, the van der Waals–London dispersion interaction is much richer than in the case of simple isotropic systems. The anisotropy of dielectric response leads straightforwardly to orientation-dependent interactions and the van der Waals–London dispersion torques, which can, in turn, introduce strong alignment forces either between

SWCNTs themselves or between SWCNTs and anisotropic macroscopic substrates. These are the main focus of this paper.

Anisotropic van der Waals–London dispersion forces between SWCNTs will be analyzed in two separate, analytically tractable limits corresponding to large and small separations as compared with the radius of the SWCNTs. We refer to these as the *far* and *near* limits. The intermediate regime will be covered by sensible interpolation formulas. In the far limit, the *Parsegian method* for anisotropic cylinders will provide the basis for numerical evaluation of the vdW-Ld interaction. In the near limit, corresponding to near contact, the cylinder-surface and cylinder-cylinder geometries are, to a first-order approximation, equivalent to the infinite half-space formulations of the Lifshitz theory augmented by the *Derjaguin method* (Ref. 17 p. 204). Previously developed numerical implementations of the Lifshitz theory valid for two infinite half-spaces can, thus, be fruitfully used in this limit.

The structure of this paper is as follows: we first introduce the van der Waals–London dispersion spectrum and discuss its properties for two representative cases of the SWCNTs. We then derive the exact Lifshitz formulas for the van der Waals–London dispersion interaction energy between an optically anisotropic cylinder and a semi-infinite optically anisotropic substrate and between two optically anisotropic cylinders in both the far and near limits. We formulate the vdW-Ld interaction energies in terms of the appropriate Hamaker coefficients. We then evaluate these Hamaker coefficients for the relevant SWCNT van der Waals–London dispersion spectra and propose an interpolation formula that will cover the whole regime of separations. Finally, we will comment on and discuss the magnitude and salient properties of the van der Waals–London dispersion interaction in the context of SWCNTs.

II. DIELECTRIC AND LONDON DISPERSION SPECTRA

A. Full spectral Hamaker coefficients

In the framework of the Lifshitz theory (Ref. 17 p. 283) the nonretarded dispersion interaction free energy between two semi-infinite half-spaces is conveniently written as

$$\mathcal{G}(\ell) = -\frac{A_{123}}{12\pi\ell^2} \tag{1}$$

with a Hamaker coefficient defined in this case as

$$A_{123} = -6kT\ell^2 \sum_{n=0}^{\infty}{}' \int_0^{\infty} Q dQ \ln[1 - \Delta_{32}(\xi_n)\Delta_{12}(\xi_n)e^{-2Q\ell}]$$

$$\simeq \frac{3}{2}k_B T \sum_{n=0}^{\infty}{}' \Delta_{12}(\xi_n)\Delta_{23}(\xi_n). \tag{2}$$

Here, 1 and 3 (of 123) represent the left and right infinite half-space materials separated by medium 2 of thickness ℓ. Q is the magnitude of the wave vector in the plane of the two opposed interfaces. The summation in the expression above is not continuous but rather over a discrete set of Matsubara,

or boson, frequencies $\xi_n = \frac{2\pi k_B T n}{\hbar}$, where k_B is the Boltzmann constant and $\hbar$ is the Planck constant divided by 2π. At room temperature, this interval per n is approximately 0.16 eV. The prime in the summation signifies that the first, $n=0$, term is taken with weight $\frac{1}{2}$.

The Hamaker coefficient depends on the values of Δ's that describe the relative dielectric mismatches between the dielectric media involved in the interaction and are defined as

$$\Delta_{kj}(\xi_n) = \frac{\epsilon_k(i\xi_n) - \epsilon_j(i\xi_n)}{\epsilon_k(i\xi_n) + \epsilon_j(i\xi_n)}. \tag{3}$$

The dielectric function at imaginary values of the frequency argument, which is obviously the fundamental ingredient of the Lifshitz theory of van der Waals interactions, can be obtained via the Kramers-Kronig (KK) transform in the form

$$\epsilon(i\xi) = 1 + \frac{2}{\pi}\int_0^{\infty} \frac{\epsilon''(\omega)d\omega}{\omega^2 + \xi^2}, \tag{4}$$

where $\epsilon''(\omega)$ is the imaginary part of the dielectric response function, i.e., $\epsilon(\omega) = \epsilon'(\omega) + i\epsilon''(\omega)$. $\epsilon(i\xi)$ is referred to as the *van der Waals–London dispersion spectrum* (or vdW-Ld spectrum). The magnitude of $\epsilon(i\xi)$ essentially describes how well the material responds and is polarized by fluctuations up to the given frequency. Note that the integration in Eq. (4) requires frequencies out to infinity. In practice this is impossible, but also unnecessary, as long as all the interband transition energies are either known or properly approximated.

For simple systems, it may be acceptable to use this simple formulation for planar geometries to get a general feel for the magnitude and sign of the Hamaker coefficient. However, the geometry of the system cannot be ignored at certain distances and in certain arrangements and must be taken into account.

B. Structure and optical properties

In order to obtain accurate vdW-Ld spectra over a sufficiently large frequency range (as large as possible while maintaining accuracy), *ab initio* electronic structure codes were used to calculate $\epsilon''(\omega)$ from the resulting band structure via its connection with the dipolar transition strengths $\langle kn\sigma|p_i|kn'\sigma\rangle$ of the form[18]

$$\epsilon''_{ij}(\omega) = \frac{4\pi^2 e^2}{\Omega m^2\omega^2} \sum_{knn'\sigma} \langle kn\sigma|p_i|kn'\sigma\rangle\langle kn'\sigma|p_j|kn\sigma\rangle f_{kn}$$

$$\times (1 - f_{kn'})\delta(e_{kn'} - e_{kn} - \hbar\omega). \tag{5}$$

Here, again $\epsilon''(\omega)$ is the imaginary part of the dielectric spectrum at a given frequency ω, with mass m and Brillouin-zone volume Ω. The momentum operators, p_i and p_j, operate on both the valence- and conduction-band wave functions, where the i and j subscripts represent the directions of the tensor in three-dimensional space. The Fermi function (f_{kn}) terms ensure that only transitions between an occupied valence to an unoccupied conduction-band transition are al-
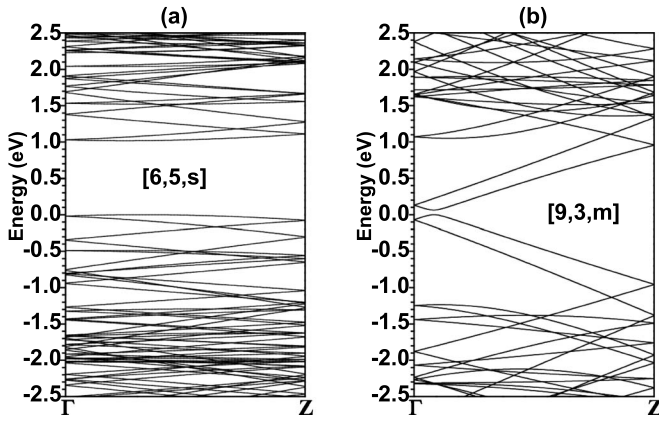
FIG. 1. The band diagrams for the axial direction of the (a) $[6,5,s]$ and (b) $[9,3,m]$ SWCNTs.

lowed, and the delta function ensures that only transitions corresponding to the particular energy $\hbar\omega$ are considered. Once $\epsilon''(\omega)$ is obtained, it is then trivial to use the Kramers-Kronig transform Eq. (4) to convert these data into a form useful for dispersion interaction computation.

Figure 1 shows the band diagrams for the $[6,5,s]$ and $[9,3,m]$ SWCNTs, which served as the basis for Eq. (5). The calculation was done for an infinitely long uncapped SWCNT (i.e., we used a single unit cell and applied periodic boundary conditions in the axial direction). The small gap present in the $[9,3,m]$ is consistent with previous research for achiral SWCNTs.[6] For practical electronic conduction purposes, it still behaves like a metal and thus it maintains its label as such. The band gap for the $[6,5,s]$ is just over 1.0 eV and is thus in agreement with previous trend analysis.[14]

Figure 2 shows the ϵ'' data for the $[6,5,s]$ and $[9,3,m]$ SWCNTs, which have identical peaks and features in comparison to the data used in our first analysis.[13] However, the magnitudes have now been scaled to compensate for the excess volume surrounding the SWCNT in the three-dimensional supercell of the orthogonalized linear combination of atomic orbitals (OLCAO) calculation so as to report the ϵ'' data of a SWCNT as a solid cylinder.[7] This scaling of the ϵ'' from that of a solid cylinder in an empty box to the solid cylinder by itself is based on the oscillator strength, or f-sum rule,[20] which relates the optical property ϵ'' to a material's electron density as follows:
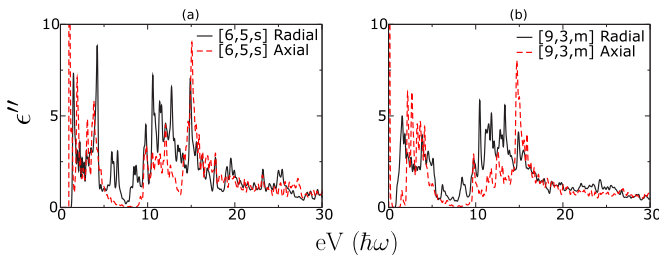
FIG. 2. (Color online) The ϵ_2 or imaginary part of the dielectric spectrum versus frequency for the (a) $[6,5,s]$ and (b) $[9,3,m]$ SWCNTs. The axial direction of the $[6,5,s]$ spikes and plateaus to values around 17 in the range of $1.00-1.07$ eV, while the $[9,3,m]$ spikes sharply up to a value of 933 at 0.04 eV.

$$n_{eff}(\omega) = \frac{m}{2\pi^2 e^2} \int_0^\omega \omega' \epsilon(\omega') d\omega'. \qquad (6)$$

Here, $n_{eff}(\omega)$ is the effective number of electrons per volume contributing to the optical properties for energy excitations up to frequency ω. Variables m and e are the standard values of electron mass and charge, respectively. For our particular system, we define the outer surface of the solid cylinder to be half a graphite interlayer spacing ($d_0/2 = 0.168$ nm),[19] beyond what is traditionally called the SWCNT radius (the traditionally defined radius is typically the distance between where the carbon nuclei reside and the center of the cylinder). We chose this extended radius because we are interested in the vdW-Ld energies and forces between two SWCNTs up until actual contact. d_0 is a suitable distance because it is the equilibrium distance between two graphene layers in graphite and also of the different layers in a multi-walled carbon nanotube system. Therefore, for an infinitely long SWCNT with its axial direction along the z direction, the scale factor is simply $xyz \big/ \pi z (r + 1/2 d_0)^2$.

The axial directions z cancel out as expected. Variables x and y represent the supercell box dimensions for the OLCAO calculation along the radial component directions of the SWCNTs. Their sizes are arbitrarily chosen to be large enough to prevent the SWCNT from feeling the effects of an identical neighbor. For both of our SWCNT calculations, we used 2 nm for the x and y dimensions and a single lattice unit translation for the z dimension (1.535 96 nm for the $[9,3,m]$ and 4.063 78 nm for the $[6,5,s]$).

As with our previous analysis, the ϵ'' data were obtained to be 30 eV. This upper limit is sufficient for most SWCNTs, as they are made of carbon and do not exhibit any of the higher-order d and f shell transitions. The two SWCNTs have noticeable differences in their ϵ'' absorption peaks between the two chiralities and between the different principal directions of a particular SWCNT. This lays the fundamental groundwork for these differences to carry over to the vdW-Ld interactions that will, thus, exhibit strong anisotropy in the interaction.

Figure 3 shows the vdW-Ld curves of water and the $[9,3,m]$ and $[6,5,s]$ tubes after the KK transform. Again, it is clear that these curves are all different, some more substantially than others. The metallic $[9,3,m]$ tube has very obvious directional dependence, with the axial direction having a large wing at low frequencies and a dampened response at high frequencies if compared to the radial vdW-Ld spectrum. To those not used to vdW-Ld spectra analysis, the SWCNT curves may look different by only 10%–20% in any given frequency regime, but these seemingly small shifts can have a big impact because of the infinite Matsubara frequency summation in Eq. (2). Small shifts in vdW-Ld spectra can even determine whether an interaction is attractive or repulsive for a multicomponent system.[21–23]

III. van der WAALS–LONDON DISPERSION INTERACTION BETWEEN ANISOTROPIC BODIES

In this section, we derive the nonretarded van der Waals–London interaction between a semi-infinite anisotropic sub-
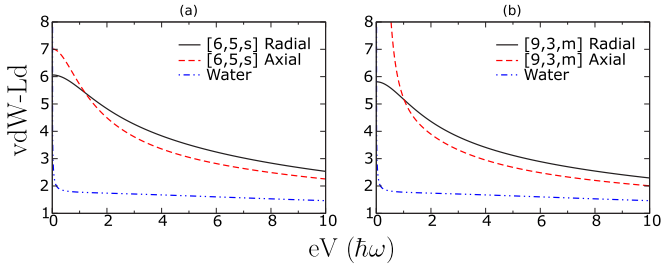
FIG. 3. (Color online) The vdW-Ld curves of both SWCNTs in their radial and axial directions for the (a) $[6,5,s]$ and (b) $[9,3,m]$ SWCNTs. The vdW-Ld spectra for water rises sharply to 78 at 0 eV, while the $[9,3,m]$ goes even higher and peaks at approximately 333.

strate and an anisotropic cylinder in two limits: the far limit, corresponding to a large l (note that l is the separation between the surface of the substrate and the surface of the cylinder), and the near limit, corresponding to the Derjaguin limit valid in the case of small separation from the substrate. The substrate is assumed to be optically uniaxial and have a dielectric response function $\epsilon_\parallel$ in the direction parallel to the surface and $\epsilon_\perp$ in the other two directions. The cylinder is also uniaxial with dielectric response functions $\epsilon^c_\parallel$ and $\epsilon^c_\perp$ parallel and perpendicular to the cylinder axis.

The philosophy of our approach is based on consecutive application of the *Parsegian method* and the *Pitaevskii method* for two semi-infinite anisotropic media (Ref. 17 p. 236):

(1) In the cylinder-substrate case, we first formulate the Lifshitz interaction energy for two plane-parallel semi-infinite anisotropic media and then use the Pitaevskii method to extract an interaction free energy between a single anisotropic cylinder and a semi-infinite anisotropic substrate. The limiting procedure of going from the anisotropic composite to a single long anisotropic cylinder is based on the application of the Parsegian method of composite anisotropic media.

(2) In the cylinder-cylinder case, we start again from the Lifshitz interaction energy for two plane-parallel semi-infinite anisotropic media but then use the Parsegian method of composite anisotropic media for both of them. Applying the Pitaevskii method to both media now allows for an extraction of the interaction free energy between two anisotropic cylinders.

For the first case listed above, a related computation was performed in a nevertheless unrelated context by Chun *et al.*[24] The main difference between this approach and the one described in detail here is that we have now circumvented all linearization assumptions, and thus our formulas are exact to all orders in the orientational dependence, we have derived the interaction formulas for any value of the substrate anisotropy, and we have used the Pitaevskii method to go from the slab-slab interaction to the cylinder-substrate interaction.

We first calculate the Lifshitz interaction free energy for two anisotropic media $\mathcal{L}$ and $\mathcal{R}$ across m of thickness ℓ in the nonretarded limit.[25] We introduce two components of the uniaxial dielectric response of the substrate $\mathcal{L}$ as $\epsilon_\parallel$ and $\epsilon_\perp$, and $\overline{\epsilon_\parallel}$ and $\overline{\epsilon_\perp}$ as the two components of the uniaxial dielectric response of the substrate $\mathcal{R}$.
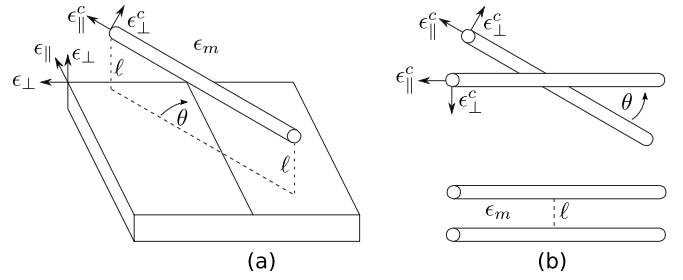
FIG. 4. Schematic showing the geometry of the (a) anisotropic cylinder–anistropic planar substrate and (b) anisotropic cylinder–anisotropic cylinder systems.

The angle between the two principal axes of media $\mathcal{L}$ and $\mathcal{R}$ is defined as θ, see Fig. 4. ϵ_m is the dielectric response of the isotropic medium between the two semi-infinite substrates. ϕ is an integration variable used to capture the interactions between all possible directions within the plane normal to the stacking direction. The interaction free energy for this system is given by the following expression (Ref. 17, p. 320)

$$G(\ell, \theta) = \frac{k_B T}{4\pi^2} {\sum_{n=0}^{\infty}}' \int_0^{2\pi} d\phi \int_0^y Q dQ \log[1 - \Delta_{\mathcal{L}m}(\phi)$$
$$\times \Delta_{\mathcal{R}m}(\theta - \phi) e^{-2Q\ell}]. \quad (7)$$

All the dielectric functions have to be taken as their Kramers-Kronig transforms at $i\xi_n$, i.e., $\epsilon(i\xi_n)$, where $\xi_n = 2\pi n \frac{k_B T}{\hbar}$. Q is the magnitude of the wave vector in the plane of the two opposed interfaces. Also here,

$$\Delta_{\mathcal{L}m}(\phi) = \frac{\epsilon_\perp \sqrt{1 + \gamma \cos^2 \phi} - \epsilon_m}{\epsilon_\perp \sqrt{1 + \gamma \cos^2 \phi} + \epsilon_m}, \quad (8)$$

where medium $\mathcal{L}$ anisotropy is defined as

$$\gamma = \frac{\epsilon_\parallel - \epsilon_\perp}{\epsilon_\perp}. \quad (9)$$

If the substrate $\mathcal{L}$ is isotropic, then $\epsilon_\parallel = \epsilon_\perp$ and $\gamma = 0$. For the medium $\mathcal{R}$, we analogously have

$$\Delta_{\mathcal{R}m}(\theta - \phi) = \frac{\overline{\epsilon_\perp} \sqrt{1 + \bar{\gamma} \cos^2(\theta - \phi)} - \epsilon_m}{\overline{\epsilon_\perp} \sqrt{1 + \bar{\gamma} \cos^2(\theta - \phi)} + \epsilon_m}, \quad (10)$$

with an anisotropy of

$$\bar{\gamma} = \frac{\overline{\epsilon_\parallel} - \overline{\epsilon_\perp}}{\overline{\epsilon_\perp}}. \quad (11)$$

Again, if the substrate $\mathcal{R}$ is isotropic, then $\overline{\epsilon_\parallel} = \overline{\epsilon_\perp}$ and $\bar{\gamma} = 0$. The interaction free energy $G(\ell, \theta)$ [Eq. (8)], can be evaluated at any separation ℓ between the interfaces of $\mathcal{L}$ and $\mathcal{R}$ as well as at any angle θ between the two principal axes of media $\mathcal{L}$ and $\mathcal{R}$.

A. Cylinder–planar substrate interaction

In order to get the interaction free energy between an anisotropic cylinder and an anisotropic substrate, we use the

Parsegian method; i.e., we assume that one of the semi-infinite substrates, i.e., $\mathcal{R}$, is a composite composed of oriented anisotropic cylinders at volume fraction v, with $\epsilon_\perp^c$ and $\epsilon_\parallel^c$ as the transverse and longitudinal dielectric response functions of the cylinder material. For the semi-infinite composite medium of oriented anisotropic cylinders $\mathcal{R}$, the anisotropic bulk dielectric response function can be derived in the form (Ref. 17 p. 318)

$$\overline{\epsilon}_\parallel = \epsilon_m(1 + v\Delta_\parallel), \quad \overline{\epsilon}_\perp = \epsilon_m\left(1 + \frac{2v\Delta_\perp}{1 - v\Delta_\perp}\right), \quad (12)$$

where

$$\Delta_\perp = \frac{\epsilon_\perp^c - \epsilon_m}{\epsilon_\perp^c + \epsilon_m}, \quad \Delta_\parallel = \frac{\epsilon_\parallel^c - \epsilon_m}{\epsilon_m}, \quad (13)$$

and ϵ_m is, again, the dielectric function of the isotropic medium between cylinders as well as between regions $\mathcal{L}$ and $\mathcal{R}$.

We now apply the Pitaevskii method to this composite system, which allows us to extract the interaction between a *single* anisotropic cylinder and a semi-infinite anisotropic substrate from an interaction energy between *two* semi-infinite substrates, of which one is a composite defined above. We start from the free energy of interaction $G(\ell, \theta)$ [Eq. (8)] where the composite of uniaxial cylinders is at a volume fraction $v = N\pi a^2$, where N is the cross-sectional number density and a is the radius of the cylinders. For this case, one can derive that (Ref. 17 p. 236)

$$-\frac{\partial G(\ell, \theta)}{\partial \ell}\bigg|_\ell = Ng(\ell, \theta). \quad (14)$$

Here, $g(\ell, \theta)$ is the interaction free energy *per unit length* between a cylinder with $a/\ell \to 0$ and a semi-infinite substrate $\mathcal{L}$, while $G(\ell, \theta)$ is the interaction free energy *per unit surface area* between a semi-infinite region $\mathcal{L}$ and a semi-infinite composite region $\mathcal{R}$, at separation ℓ and angle θ, composed of parallel anisotropic cylinders embedded in medium m. $g(\ell, \theta)$ is thus obtained by expanding $G(\ell)$ to the first order in v. This is the essence of the Pitaevskii method.

1. Far limit

We formally define the far limit as the limit $a/\ell \to 0$ and use the result of the previous section to explicitly derive $g(\ell, \theta)$. In order to use the Pitaevskii method, we expand $\Delta_{\mathcal{R}m}(\theta - \phi)$ to lowest order in v,

$$\Delta_{\mathcal{R}m}(\theta - \phi) = -\left[\Delta_\perp + \frac{1}{4}(\Delta_\parallel - 2\Delta_\perp)\cos^2(\theta - \phi)\right]v + \mathcal{O}(v^2). \quad (15)$$

To this order in v, the Q integral in Eq. (8) can then be done explicitly

$$G(\ell, \theta) = -\frac{k_BT}{16\pi^2\ell^2}v\sum_{n=0}^{\infty}{}' \int_0^{2\pi} d\phi\Delta_{\mathcal{L}m}(\phi)$$

$$\times\left[\Delta_\perp + \frac{1}{4}(\Delta_\parallel - 2\Delta_\perp)\cos^2(\theta - \phi)\right]. \quad (16)$$

Now apply Eq. (15) and thus extract the interaction free energy per unit length of a cylinder

$$g(\ell, \theta) = -\frac{k_BT\pi a^2}{4\pi^2 2\ell^3}\sum_{n=0}^{\infty}{}' \int_0^{2\pi} d\phi\Delta_{\mathcal{L}m}(\phi)$$

$$\times\left[\Delta_\perp + \frac{1}{4}(\Delta_\parallel - 2\Delta_\perp)\cos^2(\theta - \phi)\right]. \quad (17)$$

Integration over ϕ leads to a term that is independent of θ plus a term that goes as $\cos^2\theta$. This can be proved simply by Taylor expanding the above equation in $\cos^2\phi$ and evaluating the ϕ integrals order by order. This is tedious but straightforward. Therefore we can write $g(\ell, \theta)$ in the compact form

$$g(\ell, \theta) = -\frac{k_BT(\pi a^2)}{4\pi\ell^3}(\mathcal{H}^{(0)} + \mathcal{H}^{(2)}\cos^2\theta). \quad (18)$$

We define $\mathcal{H}^{(0)}$ and $\mathcal{H}^{(2)}$ by picking two convenient angles θ in Eq. (18) as $\theta = 0$ and $\theta = \frac{\pi}{2}$. For $\theta = 0$,

$$\mathcal{H}^{(0)} + \mathcal{H}^{(2)} = \frac{1}{2\pi}\sum_{n=0}^{\infty}{}' \int_0^{2\pi} d\phi\Delta_{\mathcal{L}m}(\phi)$$

$$\times\left[\Delta_\perp + \frac{1}{4}(\Delta_\parallel - 2\Delta_\perp)\cos^2\phi\right], \quad (19)$$

and for $\theta = \frac{\pi}{2}$,

$$\mathcal{H}^{(0)} = \frac{1}{2\pi}\sum_{n=0}^{\infty}{}' \int_0^{2\pi} d\phi\Delta_{\mathcal{L}m}(\phi)\left[\Delta_\perp + \frac{1}{4}(\Delta_\parallel - 2\Delta_\perp)\sin^2\phi\right]. \quad (20)$$

$\mathcal{H}^{(0)}$ and $\mathcal{H}^{(2)}$ can be evaluated explicitly since all the integrals are elementary, but the expressions obtained contain various elliptic functions and are not particularly illuminating. They can be obtained easily with MATHEMATICA.

In order to cast the result in a form that can be easily evaluated and interpreted, we first define two Hamaker coefficients as

$$\mathcal{A}^{(0)} = \frac{3}{2}k_BT\mathcal{H}^{(0)} \quad \text{and} \mathcal{A}^{(2)} = \frac{3}{2}k_BT\mathcal{H}^{(2)}. \quad (21)$$

$\mathcal{A}^{(0)}$ describes the orientation-independent part of the interaction, and $\mathcal{A}^{(2)}$ the orientation-dependent part. The interaction free energy per unit length between a cylinder of radius a and a planar anisotropic substrate at surface-surface separation ℓ [Eq. (19)] becomes

$$g(\ell, \theta) = -\frac{(\pi a^2)(\mathcal{A}^{(0)} + \mathcal{A}^{(2)}\cos^2\theta)}{6\pi\ell^3}. \quad (22)$$

This is the main result that we will use in order to quantify the van der Waals–London dispersion interaction between a cylindrical CNT and an anisotropic semi-infinite substrate. Note that in Eq. (23) all the ℓ and θ dependencies are explicitly given.

For completeness, we also give the results for the force and torque on the cylinder. The force per unit length of the cylinder is thus

$$f(\ell,\theta) = -\frac{\partial g(\ell,\theta)}{\partial \ell} \qquad (23)$$

or

$$f(\ell,\theta) = -\frac{(\pi a^2)(\mathcal{A}^{(0)} + \mathcal{A}^{(2)} \cos^2\theta)}{2\pi\ell^4}. \qquad (24)$$

The corresponding torque per unit length is the derivative

$$\tau(\ell,\theta) = -\frac{\partial g(\ell,\theta)}{\partial \theta}, \qquad (25)$$

explicitly,

$$\tau(\ell,\theta) = -\frac{(\pi a^2)\mathcal{A}^{(2)} \sin 2\theta}{6\pi\ell^3}. \qquad (26)$$

These last results in the far limit give the force per unit length $f(\ell,\theta)$ and the torque per unit length $\tau(\ell,\theta)$ as a function of the separation ℓ and the angle between the two dielectric axes θ.

2. Near limit

We now investigate the opposite limit, $\ell/a \to 0$, which we term the near limit. Here, one uses the Derjaguin method to get the interaction energy of two cylinders, one of which has an infinite radius of curvature, from the interaction energy between two half-spaces. In this case, the interaction energy per unit length between cylinders of radii a_1 and a_2 can be derived as (Ref. 17, p. 204)

$$g(\ell,\theta;a_1,a_2) = \int_{-\infty}^{+\infty} G(\ell + \alpha(a_1 x)^2,\theta)a_1 dx, \qquad (27)$$

where

$$\alpha = \frac{a_1 + a_2}{2a_1 a_2}. \qquad (28)$$

The Derjaguin method Eq. (28) is based on a summation of interactions between quasiparallel sections of the two cylinders. From Eqs. (8) and (28), it follows that

$$\int_{-\infty}^{+\infty} G(\ell + \alpha x^2,\theta)d(a_1 x) = -\frac{k_B T}{4\pi^2}\sum_{n=0}^{\infty}{}' \int_0^{2\pi} d\phi \int_0^{\infty} Q dQ \Delta_{\mathcal{L}m}$$

$$\times(\phi)\Delta_{\mathcal{R}m}(\theta - \phi)e^{-2Q\ell}\int_{-\infty}^{+\infty}$$

$$\times e^{-2Q\alpha(a_1 x)^2} d(a_1 x), \qquad (29)$$

and thus,

$$g(\ell,\theta;a_1,a_2) = -\frac{k_B T}{16\ell^{3/2}}\sqrt{\frac{2a_1 a_2}{a_1 + a_2}}\sum_{n=0}^{\infty}{}' \frac{1}{2\pi}\int_0^{2\pi}$$

$$\times d\phi \Delta_{\mathcal{L}m}(\phi)\Delta_{\mathcal{R}m}(\theta - \phi). \qquad (30)$$

For the interaction between a cylinder and a plane, let $a_1 \to a$ and $a_2 \to \infty$. Also, let one of the semi-infinite slabs, again say this is $\mathcal{R}$, be composed of the anisotropic cylinder material so that

$$\Delta_{\mathcal{R}m}(\theta - \phi) = \frac{\epsilon_\perp^c \sqrt{1 + \gamma^c \cos^2(\theta - \phi)} - \epsilon_m}{\epsilon_\perp^c \sqrt{1 + \gamma^c \cos^2(\theta - \phi)} + \epsilon_m}. \qquad (31)$$

Here, again

$$\gamma^c = \frac{\epsilon_\parallel^c - \epsilon_\perp^c}{\epsilon_\perp^c}, \qquad (32)$$

and $\epsilon_\perp^c$ and $\epsilon_\parallel^c$ are the transverse and longitudinal dielectric responses of the cylinder, and ϵ_m that of the solution medium. This formula is valid for any angle between the two cylinders or, equivalently, between the two principal axes of the dielectric response: the axis of the cylinder and the principal axis of the anisotropic substrate. The angular integral is analytically solvable for any anisotropy by the same methods as used to derive Eq. (19) and leads to the interaction free energy per unit length between a cylinder and an anisotropic substrate,

$$g(\ell,\theta;a) = -\frac{k_B T \sqrt{2a}}{16\ell^{3/2}}(\mathcal{H}^{(0)} + \mathcal{H}^{(2)} \cos^2\theta). \qquad (33)$$

Here, $\mathcal{H}^{(0)}$ and $\mathcal{H}^{(2)}$ are obtained in complete analogy to Eq. (19) from

$$\mathcal{H}^{(0)} + \mathcal{H}^{(2)} = \frac{1}{2\pi}\sum_{n=0}^{\infty}{}' \int_0^{2\pi} d\phi \left(\frac{\epsilon_\perp \sqrt{1 + \gamma \cos^2\phi} - \epsilon_m}{\epsilon_\perp \sqrt{1 + \gamma \cos^2\phi} + \epsilon_m}\right)$$

$$\times \left(\frac{\epsilon_\perp^c \sqrt{1 + \gamma^c \cos^2\phi} - \epsilon_m}{\epsilon_\perp^c \sqrt{1 + \gamma^c \cos^2\phi} + \epsilon_m}\right) \qquad (34)$$

and

$$\mathcal{H}^{(0)} = \frac{1}{2\pi}\sum_{n=0}^{\infty}{}' \int_0^{2\pi} d\phi \left(\frac{\epsilon_\perp \sqrt{1 + \gamma \cos^2\phi} - \epsilon_m}{\epsilon_\perp \sqrt{1 + \gamma \cos^2\phi} + \epsilon_m}\right)$$

$$\times \left(\frac{\epsilon_\perp^c \sqrt{1 + \gamma^c \sin^2\phi} - \epsilon_m}{\epsilon_\perp^c \sqrt{1 + \gamma^c \sin^2\phi} + \epsilon_m}\right). \qquad (35)$$

In order to cast the result in an easily evaluated and interpreted form, we define Hamaker coefficients as

$$\mathcal{A}^{(0)} = \frac{3}{2}k_B T\mathcal{H}^{(0)} \quad \text{and} \quad \mathcal{A}^{(2)} = \frac{3}{2}k_B T\mathcal{H}^{(2)}. \qquad (36)$$

Coefficient $\mathcal{A}^{(0)}$ again describes the orientation-independent part of the interaction and $\mathcal{A}^{(2)}$ the orientation-dependent part of the interaction. The interaction free energy per unit length between a thick cylinder (near limit) and a planar anisotropic substrate at surface-surface separation ℓ [Eq. (34)] becomes

$$g(\ell,\theta,a) = -\frac{\sqrt{2a}(\mathcal{A}^{(0)} + \mathcal{A}^{(2)} \cos^2\theta)}{24\ell^{3/2}}. \qquad (37)$$

This is the second main result that we will use in order to quantify the van der Waals–London dispersion interaction between a cylindrical CNT and an anisotropic semi-infinite substrate at close separations. Note that here, too, all the ℓ and θ dependencies are explicitly given.

The corresponding force per unit length is then according to Eq. (24)

$$f(\ell,\theta,a) = -\frac{\partial g(\ell,\theta,a)}{\partial \ell} \tag{38}$$

or

$$f(\ell,\theta,a) = -\frac{\sqrt{2a}(\mathcal{A}^{(0)} + \mathcal{A}^{(2)}\cos^2\theta)}{16\ell^{5/2}}. \tag{39}$$

The torque per unit length is then again

$$\tau(\ell,\theta,a) = -\frac{\partial g(\ell,\theta,a)}{\partial \theta} \tag{40}$$

or, explicitly,

$$\tau(\ell,\theta,a) = -\frac{\sqrt{2a}\mathcal{A}^{(2)}\sin 2\theta}{24\ell^{3/2}}. \tag{41}$$

This completes the near limit for the interaction free energy per unit length $g(\ell,\theta,a)$ in the cylinder–planar substrate system as an explicit function of the surface separation ℓ and the angle θ between the two principal dielectric axes.

B. Cylinder-cylinder interaction

In order to get the interaction free energy between two anisotropic cylinders, we again use the Parsegian method, assuming now that both $\mathcal{L}$ and $\mathcal{R}$ are composites composed of oriented anisotropic cylinders at volume fraction v, with $\epsilon_\perp^c$ and $\epsilon_\parallel^c$ as the transverse and longitudinal dielectric response functions of the cylinder material. The rest of the derivation is very similar to the case of the cylinder and a semi-infinite substrate. We again decompose it into the far and near limits.

1. Far limit

Start with the interaction between two semi-infinite media, both composed of uniaxial cylinders at a volume fraction $v = N\pi a^2$, where N is the cross-sectional number density and a is the radius of the cylinders.

Depending on θ, in this case, Eq. (15) comes in two variants. If the cylinders in each of the composite media are parallel, $\theta = 0$, then (Ref. 15 p. 234)

$$\frac{d^2\mathcal{G}(\ell,\theta=0)}{d\ell^2} = N^2 \int_{-\infty}^{+\infty} g(\sqrt{\ell^2 + y^2})dy. \tag{42}$$

Here, $g(\ell)$ is the free energy of interaction between parallel cylinders per unit length at a separation ℓ. If, on the other hand, the angle θ is finite, i.e., $\theta \neq 0$, then the corresponding expression becomes (Ref. 17, p. 234)

$$\frac{d^2\mathcal{G}(\ell,\theta)}{d\ell^2} = N^2 \sin\theta[G(\ell,\theta)]. \tag{43}$$

Here, $G(\ell,\theta)$ is the interaction free energy between the two cylinders, skewed at an angle θ. For two semi-infinite composite media, Eq. (3) now becomes

$$\mathcal{G}(\ell,\theta) = \frac{k_B T}{4\pi^2}\sum_{n=0}^{\infty}{}' \int_0^{2\pi} d\phi \int_0^y QdQ \log$$
$$\times [1 - \Delta_{\mathcal{L}m}(\phi)\Delta_{\mathcal{R}m}(\theta - \phi)e^{-2Q\ell}], \tag{44}$$

where

$$\Delta_{\mathcal{L}m}(\phi) = \frac{\overline{\epsilon_\perp(\mathcal{L})}\sqrt{1 + \overline{\gamma(\mathcal{L})}\cos^2\phi} - \epsilon_m}{\overline{\epsilon_\perp(\mathcal{L})}\sqrt{1 + \overline{\gamma(\mathcal{L})}\cos^2\phi} + \epsilon_m}. \tag{45}$$

and

$$\Delta_{\mathcal{R}m}(\theta-\phi) = \frac{\overline{\epsilon_\perp(\mathcal{R})}\sqrt{1 + \overline{\gamma(\mathcal{R})}\cos^2(\theta-\phi)} - \epsilon_m}{\overline{\epsilon_\perp(\mathcal{R})}\sqrt{1 + \overline{\gamma(\mathcal{R})}\cos^2(\theta-\phi)} + \epsilon_m}. \tag{46}$$

We have kept the option that the two cylinders are composed of different materials, $(\mathcal{R})$ and $(\mathcal{L})$. The other definitions are trivially generalized, for $(\mathcal{R})$ and $(\mathcal{L})$, from

$$\overline{\gamma} = \frac{\overline{\epsilon_\parallel} - \overline{\epsilon_\perp}}{\overline{\epsilon_\perp}}, \tag{47}$$

with

$$\overline{\epsilon_\parallel} = \epsilon_m(1 + v\Delta_\parallel), \quad \overline{\epsilon_\perp} = \epsilon_m\left(1 + \frac{2v\Delta_\perp}{1 - v\Delta_\perp}\right), \tag{48}$$

where

$$\Delta_\perp \equiv \frac{\epsilon_\perp^c - \epsilon_m}{\epsilon_\perp^c + \epsilon_m}, \quad \Delta_\parallel \equiv \frac{\epsilon_\parallel^c - \epsilon_m}{\epsilon_m}. \tag{49}$$

Starting first with the expansion of $\Delta_{\mathcal{R}m}$ and $\Delta_{\mathcal{L}m}$ in terms of v,

$$\Delta_{\mathcal{L}m}(\phi) = -\left\{\Delta_\perp(\mathcal{L}) + \frac{1}{4}[\Delta_\parallel(\mathcal{L}) - 2\Delta_\perp(\mathcal{L})]\cos^2\phi\right\}v$$
$$+ \mathcal{O}(v^2),$$

$$\Delta_{\mathcal{R}m}(\phi) = -\left\{\Delta_\perp(\mathcal{R}) + \frac{1}{4}[\Delta_\parallel(\mathcal{R}) - 2\Delta_\perp(\mathcal{R})]\cos^2(\theta-\phi)\right\}v$$
$$+ \mathcal{O}(v^2). \tag{50}$$

To second order in v, this gives

$$\mathcal{G}(\ell,\theta) = -\frac{k_B T}{2\pi}N^2(\pi a^2)^2\sum_{n=0}^{\infty}{}'$$
$$\times(\mathcal{H}^{(0)} + \mathcal{H}^{(2)}\cos^2\theta)\int_0^\infty QdQe^{-2Q\ell} \tag{51}$$

by using $v = N(\pi a^2)$. Here,

$$\mathcal{H}^{(0)} + \mathcal{H}^{(2)} = \frac{1}{2\pi}\int_0^{2\pi}$$

$$\times d\phi\left\{\Delta_\perp(\mathcal{L}) + \frac{1}{4}[\Delta_\parallel(\mathcal{L}) - 2\Delta_\perp(\mathcal{L})]\cos^2\phi\right\}$$

$$\times\left\{\Delta_\perp(\mathcal{R}) + \frac{1}{4}[\Delta_\parallel(\mathcal{R}) - 2\Delta_\perp(\mathcal{R})]\cos^2\phi\right\} \quad (52)$$

and

$$\mathcal{H}^{(0)} = \frac{1}{2\pi}\int_0^{2\pi} d\phi\left\{\Delta_\perp(\mathcal{L}) + \frac{1}{4}[\Delta_\parallel(\mathcal{L}) - 2\Delta_\perp(\mathcal{L})]\cos^2\phi\right\}$$

$$\times\left\{\Delta_\perp(\mathcal{R}) + \frac{1}{4}[\Delta_\parallel(\mathcal{R}) - 2\Delta_\perp(\mathcal{R})]\sin^2\phi\right\}. \quad (53)$$

We can now extract interaction formulas for a pair of skewed or parallel cylinders. In the simpler skewed case, Eqs. (44) and (52) give

$$\sin\theta[G(\ell,\theta)] = -\frac{k_B T}{2\pi}(\pi a^2)^2 4\sum_{n=0}^{\infty}{}'(\mathcal{H}^{(0)} + \mathcal{H}^{(2)}\cos^2\theta)\int_0^\infty Q^3 dQ e^{-2Q\ell} \quad (54)$$

or

$$G(\ell,\theta) = -\frac{3k_B T(\pi a^2)^2}{4\pi\ell^4\sin\theta}\sum_{n=0}^{\infty}{}'(\mathcal{H}^{(0)} + \mathcal{H}^{(2)}\cos^2\theta). \quad (55)$$

Introducing two Hamaker coefficients

$$\mathcal{A}^{(0)} = \frac{3}{2}k_B T\mathcal{H}^{(0)} \quad \text{and} \quad \mathcal{A}^{(2)} = \frac{3}{2}k_B T\mathcal{H}^{(2)}, \quad (56)$$

we can write the interaction free energy between two thin cylinders (far limit) of radius a skewed at an angle θ and at a (smallest) separation ℓ in the form

$$G(\ell,\theta) = -\frac{(\pi a^2)^2(\mathcal{A}^{(0)} + \mathcal{A}^{(2)}\cos^2\theta)}{2\pi\ell^4\sin\theta}. \quad (57)$$

Note that this is now a total interaction free energy and *not* interaction free energy per unit length. This is the third main result that we will use in order to quantify the van der Waals–London dispersion interaction between two cylindrical CNTs at large separations. Note, too, that all the ℓ and θ dependencies are explicitly given.

For completeness, we also derive the expressions for the force and the torque. The corresponding force is again obtained from

$$f(\ell,\theta) = -\frac{\partial G(\ell,\theta)}{\partial\ell} \quad (58)$$

or

$$f(\ell,\theta) = -\frac{2(\pi a^2)^2(\mathcal{A}^{(0)} + \mathcal{A}^{(2)}\cos^2\theta)}{\pi\ell^5\sin\theta}. \quad (59)$$

Similarly, the torque is

$$\tau(\ell,\theta) = -\frac{\partial G(\ell,\theta)}{\partial\theta} \quad (60)$$

or

$$\tau(\ell,\theta) = -\frac{(\pi a^2)^2}{2\pi\ell^4}\left[\frac{\mathcal{A}^{(0)}}{\sin^2\theta} + \mathcal{A}^{(2)}(2 + \cot^2\theta)\right]\cos\theta. \quad (61)$$

For parallel cylinders, the derivation proceeds along a different line, since now the interaction energy scales proportional to the total length of the cylinders. Starting with Eq. (43) gives

$$\int_{-\infty}^{+\infty} g(\sqrt{\ell^2 + y^2})dy = -\frac{k_B T}{2\pi}(\pi a^2)^2 4\sum_{n=0}^{\infty}{}'(\mathcal{H}^{(0)} + \mathcal{H}^{(2)})\int_0^\infty Q^3 dQ e^{-2Q\ell}. \quad (62)$$

By the inverse Abel transform,

$$h(\ell) = \int_{-\infty}^{+\infty} g(\ell^2 + y^2)dy \rightarrow g(\ell) = -\frac{1}{\pi}\int_\ell^\infty\frac{h'(y)dy}{\sqrt{\ell^2 - y^2}}, \quad (63)$$

we obtain

$$g(\ell) = -\frac{1}{\pi}\frac{k_B T}{2\pi}(\pi a^2)^2 8\sum_{n=0}^{\infty}{}'(\mathcal{H}^{(0)} + \mathcal{H}^{(2)})\int_0^\infty Q^3 dQ K_0(-2Q\ell) \quad (64)$$

by using the standard identity

$$\int_\ell^\infty\frac{e^{-2Qy}dy}{\sqrt{\ell^2 - y^2}} = K_0(-2Q\ell). \quad (65)$$

From here, it is easy to write explicitly the interaction free energy per unit length between two parallel cylinders of radius a,

$$g(\ell) = -\frac{9k_B T(\pi a^2)^2}{16\pi\ell^5}\sum_{n=0}^{\infty}{}'(\mathcal{H}^{(0)} + \mathcal{H}^{(2)}). \quad (66)$$

The Matsubara sum $\sum_{n=0}^{\infty}{}'$ is as before. With the two Hamaker coefficients

$$\mathcal{A}^{(0)} = \frac{3}{2}k_B T\mathcal{H}^{(0)} \quad \text{and} \quad \mathcal{A}^{(2)} = \frac{3}{2}k_B T\mathcal{H}^{(2)}, \quad (67)$$

we remain with

$$g(\ell) = -\frac{3(\pi a^2)^2(\mathcal{A}^{(0)} + \mathcal{A}^{(2)})}{8\pi\ell^5}. \quad (68)$$

This is the free energy of interaction between two parallel thin cylinders at a separation ℓ in the far limit. This is the fourth main result that we will use in order to quantify the

van der Waals–London dispersion interaction between two parallel cylindrical CNTs at large separations.

Again, for the sake of completeness, we quote the results for the corresponding force per unit length as

$$f(\ell, \theta) = -\frac{\partial g(\ell, \theta)}{\partial \ell} \tag{69}$$

or

$$f(\ell, \theta) = -\frac{15(\pi a^2)^2(\mathcal{A}^{(0)} + \mathcal{A}^{(2)})}{8\pi\ell^6}. \tag{70}$$

2. Near limit

In the limit of small separations between the two cylinders $\ell/a \to 0$, we reformulate the approach based on the Derjaguin method and introduced for a single cylinder and a substrate. For closely opposed curved surfaces where c_1^1, c_2^1 are the principal curvatures of surface 1 and c_1^2, c_2^2 are the principal curvatures of surface 2, the Derjaguin method leads to the interaction energy of the form (Ref. 17 p. 204)

$$G(\ell, \theta; a_1, a_2) = \int\int_{-\infty}^{+\infty} \mathcal{G}\left(\ell + \frac{1}{2}c_1x^2 + \frac{1}{2}c_2y^2\right)dx\,dy, \tag{71}$$

where c_1 and c_2 are defined as

$$c_1c_2 = (c_1^1c_2^1 + c_1^2c_2^2) + (c_1^1c_1^2 + c_2^1c_2^2)\sin^2\theta$$
$$\times + (c_1^1c_2^2 + c_1^1c_2^2)\cos^2\theta. \tag{72}$$

With polar variables, the integral Eq. (72) can be rewritten as

$$G(\ell, \theta; a_1, a_2) = \int_0^{2\pi}\int_0^{+\infty} \mathcal{G}\left(\ell + \frac{1}{2}\rho^2\right)\frac{\rho\,d\rho\,d\phi}{\sqrt{c_1c_2}}. \tag{73}$$

For two cylinders with radii a_1 and a_2 at an angle θ, the above equations can be cast in the form

$$G(\ell, \theta; a_1, a_2) = \frac{2\pi\sqrt{a_1a_2}}{\sin\theta}\int_\ell^\infty \mathcal{G}(h, \theta)dh. \tag{74}$$

This gives, to the lowest order in the Δ's,

$$G(\ell, \theta; a_1, a_2) = -\frac{\sqrt{a_1a_2}k_BT}{8\pi\ell\sin\theta}\sum_{n=0}^{\infty}{}'\int_0^{2\pi} d\phi\,\Delta_{\mathcal{L}m}(\phi)\Delta_{\mathcal{R}m}(\theta-\phi). \tag{75}$$

Taking into account Eqs. (46) and (47), the angular integral is again analytically solvable for any anisotropy and leads to the following result for the interaction free energy of two cylinders of equal radii $a_1 = a_2 = a$:

$$G(\ell, \theta; a) = -\frac{ak_BT}{4\ell\sin\theta}(\mathcal{H}^{(0)} + \mathcal{H}^{(2)}\cos^2\theta), \tag{76}$$

where $\mathcal{H}^{(0)}$ and $\mathcal{H}^{(2)}$ are obtained from

$$\mathcal{H}^{(0)} + \mathcal{H}^{(2)} = \frac{1}{2\pi}\sum_{n=0}^{\infty}{}'\int_0^{2\pi} d\phi\left(\frac{\epsilon_\perp^c(\mathcal{R})\sqrt{1 + \gamma^c(\mathcal{R})\cos^2\phi} - \epsilon_m}{\epsilon_\perp^c(\mathcal{R})\sqrt{1 + \gamma^c(\mathcal{R})\cos^2\phi} + \epsilon_m}\right)\left(\frac{\epsilon_\perp^c(\mathcal{L})\sqrt{1 + \gamma^c(\mathcal{L})\cos^2\phi} - \epsilon_m}{\epsilon_\perp^c(\mathcal{L})\sqrt{1 + \gamma^c(\mathcal{L})\cos^2\phi} + \epsilon_m}\right) \tag{77}$$

and

$$\mathcal{H}^{(0)} = \frac{1}{2\pi}\sum_{n=0}^{\infty}{}'\int_0^{2\pi} d\phi\left(\frac{\epsilon_\perp^c(\mathcal{R})\sqrt{1 + \gamma^c(\mathcal{R})\cos^2\phi} - \epsilon_m}{\epsilon_\perp^c(\mathcal{R})\sqrt{1 + \gamma^c(\mathcal{R})\cos^2\phi} + \epsilon_m}\right)$$
$$\times\left(\frac{\epsilon_\perp^c(\mathcal{L})\sqrt{1 + \gamma^c(\mathcal{L})\sin^2\phi} - \epsilon_m}{\epsilon_\perp^c(\mathcal{L})\sqrt{1 + \gamma^c(\mathcal{L})\sin^2\phi} + \epsilon_m}\right). \tag{78}$$

For two identical cylinders, the $\mathcal{L}$ and $\mathcal{R}$ values are the same. Again, we omit writing the explicit frequency dependence of all the dielectric functions. This dependence should be entered when numerical calculations are performed.

As above, we now introduce the Hamaker coefficients according to the definitions

$$\mathcal{A}^{(0)} = \frac{3}{2}k_BT\mathcal{H}^{(0)} \quad \text{and} \quad \mathcal{A}^{(2)} = \frac{3}{2}k_BT\mathcal{H}^{(2)}, \tag{79}$$

and thus obtain for the interaction free energy of the two cylinders of equal radii $a_1 = a_2 = a$

$$G(\ell, \theta; a) = -\frac{a}{6\ell\sin\theta}(\mathcal{A}^{(0)} + \mathcal{A}^{(2)}\cos^2\theta). \tag{80}$$

This is the final expression for the interaction free energy between two CNTs at a general angle θ and separation ℓ in the near limit. Note again that all the ℓ and θ dependencies are given explicitly. Again, for completeness, the corresponding force is given by

$$f(\ell, \theta; a) = -\frac{\partial G(\ell, \theta; a)}{\partial \ell} \tag{81}$$

or

$$f(\ell, \theta; a) = -\frac{a}{6\ell^2\sin\theta}(\mathcal{A}^{(0)} + \mathcal{A}^{(2)}\cos^2\theta). \tag{82}$$

The corresponding torque is obtained straightforwardly as

$$\tau(\ell, \theta; a) = -\frac{\partial G(\ell, \theta; a)}{\partial \theta}, \tag{83}$$

which can be rewritten as

$$\tau(\ell, \theta; a) = -\frac{a}{6\ell^2}\left[\frac{\mathcal{A}^{(0)}}{\sin^2 \theta} + \mathcal{A}^{(2)}(2 + \cot^2 \theta)\right]\cos \theta. \tag{84}$$

These are the results for two near cylinders at a surface to surface separation ℓ, at a mutual angle θ, and of a common radius a. This is the fifth main result that we will use in order to quantify the van der Waals–London dispersion interaction between two cylindrical CNTs at small separations.

Examine now the interaction free energy of two identical anisotropic cylinders of radius a at zero mutual angle. In this case, the interaction free energy per unit length can be obtained in the form (Ref. [17] p. 172)

$$g(\ell, \theta = 0; a) = -\frac{k_B T \sqrt{a}}{16\ell^{3/2}}(\mathcal{H}^{(0)} + \mathcal{H}^{(2)}), \tag{85}$$

where $\mathcal{H}^{(0)}$ and $\mathcal{H}^{(2)}$ are obtained in complete analogy to Eq. (19) from

$$\mathcal{H}^{(0)} + \mathcal{H}^{(2)} = \frac{1}{2\pi}\sum_{n=0}^{\infty}{}'\int_0^{2\pi}d\psi\left(\frac{\epsilon_\perp^c(\mathcal{R})\sqrt{1 + \gamma^c(\mathcal{R})\cos^2 \psi} - \epsilon_m}{\epsilon_\perp^c(\mathcal{R})\sqrt{1 + \gamma^c(\mathcal{R})\cos^2 \psi} + \epsilon_m}\right)\left(\frac{\epsilon_\perp^c(\mathcal{L})\sqrt{1 + \gamma^c(\mathcal{L})\cos^2 \psi} - \epsilon_m}{\epsilon_\perp^c(\mathcal{L})\sqrt{1 + \gamma^c(\mathcal{L})\cos^2 \psi} + \epsilon_m}\right). \tag{86}$$

Of course, for two identical cylinders, the ϵ values for $\mathcal{L}$ and $\mathcal{R}$ are the same. Introducing again the Hamaker coefficient as before, we get the interaction free energy per unit length of the parallel cylinders as

$$g(\ell, \theta = 0; a) = -\frac{\sqrt{a}}{24\ell^{3/2}}(\mathcal{A}^{(0)} + \mathcal{A}^{(2)}). \tag{87}$$

This is now the sixth and last result that we will use to quantify the van der Waals–London dispersion interaction between two parallel cylindrical CNTs at small separations.

C. Determining the full distance dependence of the van der Waals–London dispersion interaction energy

We have now derived two valuable limits for the vdW-Ld interaction free energy: for very large intersurface separations, when compared to the radius of the cylinder, and for very small intersurface separations, either in the case of a cylinder and a substrate or two cylinders. However, the final goal of this analysis is to take these two limiting expressions and their power-law dependence on the intersurface separation ℓ and glue them together sensibly to obtain vdW-Ld interactions for all distances in between the two asymptotic limits.

This is accomplished by comparing our two asymptotic results, the far and near limits, with approximate nonretarded Hamaker pairwise summation formulas that can be derived and numerically evaluated for any separation and any geometry. Though the Hamaker summation procedure is, of course, approximate, we are only really interested in its distance and orientational scaling because we have already calculated the absolute values of the Hamaker coefficients in the two limits above. We will, thus, derive approximate interpolation formulas between our two exact limiting results by comparing the distance and orientational scaling within the two limits with the Hamaker summation results. This appears to be a reasonable method that partly circumvents the very complicated case of exact evaluation of the vdW-Ld interactions for any separation and any orientation.

1. Cylinder–planar substrate interaction

The problem of interpolation in the case of the cylinder–planar substrate interaction is solved in the following way. We take the vdW-Ld interaction energy between a point particle and a semi-infinite substrate at a separation ℓ that decays as ℓ^{-3}. For a cylinder of volume (V), the Hamaker summation formula gives, for the interaction energy per unit length,

$$g(\theta, \ell, a) = -\frac{A}{L}\int_{(V)}\frac{dV}{\ell^3(V)}, \tag{88}$$

where the volume of integration (V) is over the interior of the cylinder, L is the length of the cylinder, and $\ell(V)$ stands for the separation of each point within the cylinder from the planar substrate. This integral cannot be evaluated analytically but can be easily obtained numerically. We then compare this numerical form of the Hamaker summation formula to a different analytical function consisting of the previous far and near limiting cases blended by an interpolation function. The total vdW-Ld interaction free energy per unit length of cylinder of radius a and length L, at all distances ℓ away from the planar substrate, is assumed to be of the form

$$g(\theta, \ell, a) = -\frac{\sqrt{2a}}{24\ell^{3/2}}(\mathcal{A}_N^{(0)} + \mathcal{A}_N^{(2)}\cos^2 \theta)f(\ell, \ell_0, \beta)$$
$$-\frac{(\pi a^2)}{6\pi(\ell + a)^3}(\mathcal{A}_F^{(0)} + \mathcal{A}_F^{(2)}\cos^2 \theta)[1 - f(\ell, \ell_0, \beta)]. \tag{89}$$

For consistency, we also had to measure all the distances from the center of the cylinder; hence, $\ell + a$ in the far term. The Hamaker coefficients in the first part correspond to defi-

nitions in the near limit [Eqs. (35) and (36)] and thus the index P; and in the second part, to definitions in the far limit [Eqs. (20) and (21)], thus the index D. Here, $f(\ell, \ell_0, \beta)$ is an interpolation function that we choose to be of the simple two-parameter Fermi form

$$f(\ell, \ell_0, \beta) = \frac{1}{1 + e^{\beta(\ell - \ell_0)}}, \qquad (90)$$

where ℓ_0 is the transition point and β is essentially a fade or blur factor between the two functions. The asymptotic behavior of the interpolation function is $f(\ell \to 0, \ell_0, \beta) = 1$ and $f(\ell \to \infty, \ell_0, \beta) = 0$.

2. Cylinder-cylinder interaction

For the skewed cylinder-cylinder interaction, we follow exactly the same procedure except that in this case we must consider the interaction free energy, rather than the interaction free energy per unit length. The Hamaker-summation result,

$$\mathcal{G}(\theta, \ell, a) = -A \int_{(V_1)} \int_{(V_2)} \frac{dV_1 dV_1}{\ell^6(V_1, V_2)}, \qquad (91)$$

is a bit more complicated than Eq. (89), because one has to integrate an ℓ^{-6} form over the volumes of the two interacting cylinders; the volume of integration (V_1) is over the interior of the first cylinder, the volume of integration (V_2) is over the interior of the second cylinder, and $\ell(V_1, V_2)$ stands for the separation. This integral cannot be evaluated analytically but can be easily obtained numerically. We then compare this numerical form of the Hamaker-summation formula to a different analytical function consisting of the previous far and near limiting cases blended together by the same interpolation function as used for the cylinder–planar substrate case. The total vdW-Ld interaction free energy in this case is then written as

$$\mathcal{G}(\theta, \ell, a) = -\frac{3a}{2\ell \sin \theta}(\mathcal{A}_N^{(0)} + \mathcal{A}_N^{(2)} \cos^2 \theta)f(\ell, \ell_0, \beta)$$

$$-\frac{(\pi a^2)^2}{2\pi(\ell + 2a)^4 \sin \theta}(\mathcal{A}_F^{(0)} + \mathcal{A}_F^{(2)} \cos^2 \theta)$$

$$\times [1 - f(\ell, \ell_0, \beta)]. \qquad (92)$$

The Hamaker coefficients in the first part correspond to definitions in the near limit [Eqs. (78) and (79)] and thus the index P, and in the second part to definitions in the far limit [Eqs. (53) and (54)] and thus the index D. Again, $f(\ell, \ell_0, \beta)$ is a Fermi interpolation function of the form Eq. (91), but possibly with a different set of parameters ℓ_0 and β.

The case of two parallel anisotropic cylinders at zero mutual angle is dealt with similarly. First, we construct the appropriate Hamaker summation integral for this geometry, which we compare with the suitably interpolated interaction free energy per unit length obtained from the two exact limits, just as above. The interpolated interaction energy is now
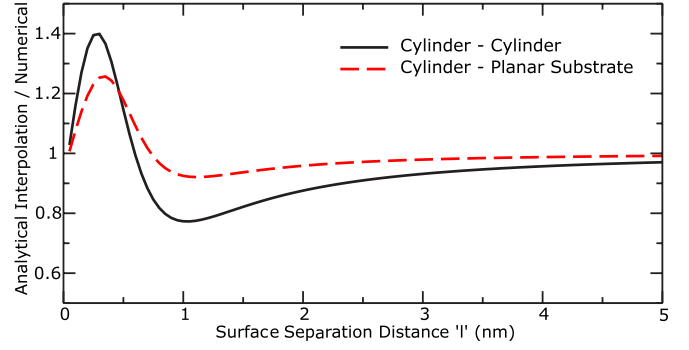
FIG. 5. (Color online) The ratio of the numerical integration [Eq. (89)] versus the interpolated analytical function [Eq. (90)] for the cylinder–planar substrate and parallel cylinder-cylinder system. The radius of the CNT cylinder in both scenarios is $a = 0.4$ nm.

$$g(\ell, a) = -\frac{\sqrt{a}}{24\pi\ell^{3/2}}(\mathcal{A}_P^{(0)} + \mathcal{A}_P^{(2)})f(\ell, \ell_0, \beta)$$

$$-\frac{3(\pi a^2)^2}{8\pi(\ell + 2a)^5}(\mathcal{A}_D^{(0)} + \mathcal{A}_D^{(2)})[1 - f(\ell, \ell_0, \beta)],$$

$$(93)$$

where the near form and the far form of the Hamaker coefficients are given by Eqs. (87) and (53), respectively. This completes the derivation of the interpolation formulas for all the cases of interaction either between a cylinder and a planar substrate or between two cylinders.

3. Numerical values of the parameters

Determining the values for ℓ_0 and β was a simple matter of fitting to obtain the best possible match. It was pleasing to discover that with simple Fermi function blending of the two analytical limiting forms we were able to capture the Hamaker-summation numerical results over all distances. Figure 5 shows the ratio of the numerical versus analytical energy for a unit length of cylinder with a 0.4 nm radius in the cylinder–planar substrate and cylinder-cylinder systems at all distances ℓ. For the cylinder–planar substrate system, we obtained $\ell_0 = 0.4$ nm and $\beta = 0.15$ as our best-fit parameters. This resulted in our interpolated interaction energy having an 8% underestimation at 1.2 nm and a 25% overestimation at approximately 0.3 nm. This is a very reasonable result considering the large change in the scale factor behavior within this small separation region. Of course, one can adjust the values of ℓ_0 and β to be more accurate in one regime versus another or change the form of the interpolation function to incorporate this small discrepancy. One important aspect of knowing this simple interpolation behavior is that it is clear which distance range is relevant to both the far and near Hamaker coefficients.

Another nice aspect regarding the interpolation function is that it is possible to get the same ratio behavior displayed in Fig. 5 for any cylinder radii by scaling the parameters β and ℓ_0 as a linear function of the cylinder radius, which is a simple consequence of the scaling form Eq. (92). For example, if we doubled the radius of the cylinder, doubling β
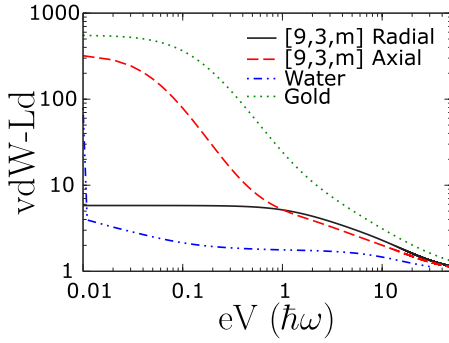
FIG. 6. (Color online) The vdW-Ld spectra of gold in comparison to water and the axial and/or radial directions of the solid cylinder [9,3,m] SWCNT spectra at low energies.

FIG. 7. (Color online) The Hamaker coefficients for both the [6,5,s] and [9,3,m] SWCNTs as a function ℓ in the case of a CNT interacting across water with a gold substrate. The ℓ_0 crossover points are equal to the solid cylinder radii ($\ell_0=a$) as described earlier. The values of the solid cylinder radii are 0.54 and 0.59 nm, respectively, for the [6,5,s] and [9,3,m] SWCNTs. The gold substrate has isotropic optical properties, so there is no dependence on the orientation of the SWCNT.

and ℓ_0 would give the curve in Fig. 5 stretched by a factor 2 along the x axis. This is very good because once we are satisfied with the curve's behavior, we know exactly how it will behave for any arbitrary CNT diameter. Therefore, for an arbitrary radius of a cylinder, the parameters $\ell_0=a$ and $\beta=0.375a$ will match the behaviors found in Fig. 5 for cylinder radii within a substantial range of variation.

For the cylinder-cylinder system, the matching between Hamaker-summation numerical and analytical interpolated solutions (Fig. 5) is acceptable given the fact that the scaling behavior change is more complicated than that for the cylinder–planar substrate system. If one needs more accuracy in this regime, they can either incorporate a more complicated interpolation function or simply use the numerical integration. However, this simple analysis is still useful for at least determining when the behavior of the system changes between the near and far limits. Our best-fit parameters for Fig. 5 were $\ell_0=0.28$ nm and $\beta=0.14$, which can also be scaled for any arbitrary cylinder radii size using $\ell_0=0.7a$ and $\beta=0.35a$.

IV. RESULTS

We now calculate the corresponding Hamaker coefficients for three main cases: a CNT interacting with an optically isotropic planar substrate, a CNT interacting with an optically anisotropic planar substrate, and two single dispersed SWCNTs interacting with each other. We will consider only cases where the CNTs are embedded in an aqueous medium because it is the most relevant in colloidal systems. The analysis can easily be extended to other media, such as air or an organic solvent, by appropriately modifying the dielectric response of the intervening medium. We also ignore the case of two optically isotropic cylinders simply because all CNTs exhibit some degree of optical anisotropy.

The gold vdW-Ld spectrum was obtained from converting frequency-dependent n and k values from experimental data in Palik[26] into ϵ'' by the relationship $\epsilon''(\omega)=n(\omega)k(\omega)$, and then transforming via the standard KK transform.[27] For the water vdW-Ld spectrum, we used the standard model composed of one Debye microwave relaxation, five Lorentz infrared relaxations, and six Lorentz ultraviolet relaxations. This relaxation model accurately captures the zero-frequency

term as well as the index of refraction in the optical frequencies (Ref. 17 p. 266). Other models for water exist,[28,29] but they either ignore the zero-frequency term or they overestimate the index of refraction. Neither of these shortcomings is trivial. For Hamaker coefficients having a magnitude less than 10 zJ in an aqueous medium, the zero-frequency term in the Lifshitz summation can be the dominating factor. For Hamaker coefficients having a magnitude of 30 zJ or higher, the values in the visible to deep UV ranges can dominate because of the large number of terms adding significantly to the summation. Therefore, we caution others to think carefully about the selection of the water dielectric spectra for a vdW-Ld interaction calculation. Figure 6 shows the gold spectra in relation to the water and solid cylinder [9,3,m] spectra.

Figure 7 shows the Hamaker coefficient for the CNT-water-gold substrate system. The total Matsubara summations contain only a single negative or *repulsive* term at $n=0$ (0 eV) for the [9,3,m] radial, [6,5,s] radial, and [6,5,s] axial directions. The rest of the terms are positive and thus lead to an overall positive Hamaker coefficient, corresponding to *attractive* nonretarded van der Waals interactions. There are three noteworthy trends in this figure: The [6,5,s]
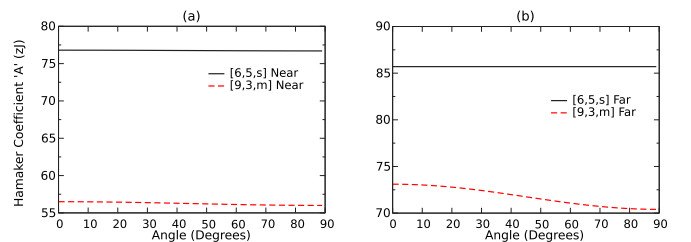
FIG. 8. (Color online) The Hamaker coefficients for both the (a) near and (b) far limits for the [6,5,s] and [9,3,m] SWCNTs as a function of orientation angle above an anisotropic substrate. The medium here is water and the anisotropic substrate is taken as a hexagonally packed array of solid SWCNT cylinders of identical chirality to the singly dispersed CNT in solution. The Hamaker coefficient is largest for $\theta=0$ (alignment).
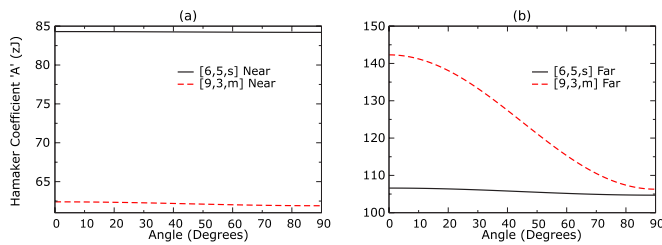
FIG. 9. (Color online) The Hamaker coefficients for two identical $[6,5,s]$ and $[9,3,m]$ SWCNTs as a function of orientation angle interacting across a water medium in the (a) near and (b) far limits. Much like the cylinder–planar substrate scenario, the magnitude of the Hamaker coefficient is maximized at $\theta=0$.

interacts more strongly with gold than the $[9,3,m]$ does in both near and far regimes, the far-limit Hamaker coefficients are larger in magnitude by $10-15$ zJ when compared to those of the near limit, and the $[9,3,m]$ has a larger spread in values between the near and far limits. The reasons behind these trends will be explained in detail in Sec. V.

Figure 8 shows the interaction across water of a CNT with a planar substrate comprised of identical chirality SWCNTs arranged in a dry hexagonal closed-packed array (volume fraction of 0.906 with air filling the void space). In this symmetric case, the vdW-Ld interaction is obviously attractive and shows a pronounced angular dependence for metallic $[9,3,m]$ in the far limit. That is, the $[9,3,m]$ Hamaker coefficients increase by 2.7 and 0.5 zJ in the far and near limits, respectively, when going from the orthogonal direction to align with the principal axis of the substrate. Conversely, the $[6,5,s]$ CNTs exhibit only negligible anisotropy in the Hamaker coefficient, gaining 0.1 zJ or less between the two orientations in both limits. Three interesting things occur in Fig. 8: The $[9,3,m]$ has more anisotropy than the $[6,5,s]$ in each limit, the anisotropy for both is greatest in the far limit, and the overall $[9,3,m]$ Hamaker coefficient is weaker than the $[6,5,s]$ in both limits.

Figure 9 shows the interaction between two CNTs of identical chirality immersed in water. We again highlight the angular dependence of the Hamaker coefficient in both regimes. Similar to the cylinder-substrate scenario, the $[9,3,m]$ interaction has a much stronger orientation dependence in the far limit, increasing in magnitude by 36 zJ or 34% when going from the orthogonal to aligned orientations. The $[6,5,s]$ Hamaker coefficient also has a notable 1.9 zJ increase in the far-limit Hamaker coefficient based solely on alignment. In the near limit, both orientation effects are much smaller, increasing by 0.5 and 0.1 zJ for the $[9,3,m]$ and $[6,5,s]$, respectively. As for trends, we again see very similar behavior to the two rod-substrate cases. The far-limit coefficients are greater in magnitude for both SWCNTs, the magnitude of the anisotropy is greatest in the far limit, and the $[9,3,m]$ Hamaker coefficient is weaker than the $[6,5,s]$ in the near limit but stronger in the far limit.

V. DISCUSSION

The importance of optical anisotropy in the context of vdW-Ld interactions between a pair of CNTs and/or between a single CNT and a planar substrate cannot be overstated. Even if only one component of the system is anisotropic, there is a need to incorporate all unique properties (in the different directions) into the consistent Lifshitz formulation. The naive approach might be to assume that we could calculate the vdW-Ld energy accurately by using both directions of the optical anisotropy separately and then averaging them in either a geometric or harmonic fashion prior to calculating the Hamaker coefficient, or attempting to calculate Hamaker constants for each direction, and averaging these by some similar method. That certainly is a possibility and might give the right phenomenology, but it is not recommended except for gaining insight into how materials of different spectra interact. The reason is that boundary conditions within the Lifshitz formulation simultaneously use both the normal and in-plane vdW-Ld spectra in order to satisfy the Maxwell equations. Therefore, it is not possible to decouple anisotropic optical properties and to think of them as a independent axial-axial or radial-radial interaction. Equation (9) shows how the integration over all values of ϕ is required within the correct Lifshitz formulation. Merely choosing the end points may result in either over- or underestimation of the Hamaker coefficient in a way that cannot be easily adjusted for all chiralities in the same manner.

Our primary focus so far[13] has been to analyze the effect of optical anisotropy rather than geometry on the overall vdW-Ld interaction. For the case of the cylinder-cylinder interaction, geometrical arrangement will play a very large role because the overall distance between the various portions of the two interacting CNTs will depend strongly on the angle of misorientation. Thus, the study of the strength of alignment forces arising from the optical properties might not seem particularly relevant compared to the geometrical effect. However, we must consider that it is, in principle, possible for two CNTs of different chiralities to have a repulsive Hamaker coefficient upon alignment that becomes attractive as they become orthogonal. To achieve repulsion, one would have to carefully select the appropriate CNTs as well as the intervening medium in order to stack the respective vdW-Ld spectra appropriately. Additionally, for the case of a planar substrate, there would be no net gain from a geometrical standpoint of rotating a CNT by any arbitrary angle. The only source of alignment would be from the anisotropic optical properties since geometry-driven alignment is no longer present. This is important if one uses anisotropic substrates to enable or enhance alignment of CNTs to a preferred direction.

Anisotropic substrates need not be packed cylinder arrays of CNTs as assumed in our analysis. We used them more out of convenience because their spectra were already available from this work and we wanted to compare the magnitude of the respective Hamaker coefficients with the cylinder-cylinder case. The problem is not so much a lack of optically anisotropic substrates, but rather a lack of accurate knowledge of their vdW-Ld spectra. It is well known that single-crystal wafers such as Al_2O_3 and SiO_2 (quartz) have directionally dependent indices of refraction[30,31] as a consequence of the directional anisotropy of the electronic band structure, just as in the case of CNTs. It nevertheless remains to be ascertained just how this anisotropy translates into the corre-

sponding frequency dependence of the vdW-Ld spectra. This dearth of accurate vdW-Ld properties will be resolved as more materials are cataloged via experimental measurement and *ab initio* calculations.

Returning to the results, we can broadly state that there are obvious differences between how CNTs interact in the three cases treated in detail in this paper (i.e., the anisotropic rod–isotropic substrate, the anisotropic rod–anisotropic substrate, and two identical anisotropic rods). We now turn to analyze the trending behavior observed in these cases in order to gain qualitative insight for future calculations involving other substrates and other CNTs. We briefly summarize them for clarity:

(1) The Hamaker coefficients in the far limit are larger in magnitude for all three systems: (a) A CNT interacting with isotropic semi-infinite substrate, (b) a CNT interacting with an anistropic semi-infinite substrate, and (c) a CNT interacting with another CNT.

(2) The $[6,5,s]$ is always stronger than the $[9,3,m]$ in the near limit, but sometimes weaker in the far limit.

(3) The far limit exhibits more anisotropic effects than the near limit. The underlying reasons for all of these are interrelated, but we will deal with each individually.

A. Importance of $\Delta_{\parallel}$ in increasing the magnitude of the far-limit Hamaker coefficients

The first trend is that the Hamaker coefficients in the far limit are always larger than the near-limit ones in any given system. Because the spectra are unchanged when going from the near to far limits, the reasons for this difference must be contained within the configurational aspects of the equations. Note that every Hamaker coefficient calculation [for example, observe Eq. (35)] has distinct components for the materials on the respective left and right sides. These terms can be thought of as spectral mismatch functions of each anisotropic spectrum interacting through the medium. If we look at both combinations of geometry (rod-substrate versus rod-rod) and both limits (near versus far), we find that rods in the far limit have mismatch functions of the form of Eq. (51) while the substrate and near-limit rod formulations have the form Eq. (9).

Note that these mismatch functions for the near-limit terms can never exceed a magnitude of 1 because they are of the form $\frac{\epsilon_L - \epsilon_m}{\epsilon_L + \epsilon_m}$ and no part of a vdW-Ld spectra can be less than 1. Thus, there is a finite limit to how much each particular term at any given Matsubara frequency n can contribute to the overall summation. However, this magnitude cap of 1 is not present for the far-limit cylinder mismatch function. Specifically, it is the $\Delta_{\parallel}$ terms [see Eq. (14)] that have the form $\frac{\epsilon_L - \epsilon_m}{\epsilon_m}$ and can easily exceed values of 1 when the medium and interacting materials have a large mismatch at any given Matsubara frequency. For example, $\Delta_{\parallel}$ for the $[9,3,m]$ peaks to a value of 18.5 at $n=1$ (approximately 0.16 eV at room temperature) and descends to 2.3 at $n=5$, while the $[6,5,s]$ averages 2.5 between $n=1$ and $n=5$. These large values of $\Delta_{\parallel}$ increase the strength of the far-limit behavior and thus explain this increase in Hamaker coefficient

magnitude in the far limit. The particularly large values for the first few frequencies of the $[9,3,m]$ summation also explains why it experiences a far greater increase in magnitude when going from the near to far limit and can therefore exceed the $[6,5,s]$ interaction strength (see Fig. 9).

B. Importance of not ignoring terms in the Lifshitz summation

One may ask why the $[6,5,s]$ would ever be larger than the $[9,3,m]$ Hamaker coefficient to begin with. The trap one may fall into is the assumption that the large wing behavior for the $[9,3,m]$ axial direction will always dominate the interaction. However, the Hamaker coefficient is, again, a summation of spectral differences over a large amount of frequencies. Those small contributions can and do add up. Although it is not obvious in Fig. 3, there is a small difference in the radial and axial direction values for all values of frequency. For example, at the frequencies around 5 eV, the $[6,5,s]$ radial direction vdW-LD spectrum is larger than the $[9,3,m]$ radial direction spectra by about 0.3. This seemingly small difference is significant enough to make all of the summation terms above $n=3$ larger for the $[6,5,s]$ SWCNT than for the $[9,3,m]$ SWCNT, resulting in a stronger overall interaction strength for the $[6,5,s]$ SWCNT.

C. How $\Delta_{\parallel}$, $\Delta_{\perp}$, and γ influence far and near-limit anisotropies

Lastly, we analyze the terms that dictate the strength of the anisotropy in the formulations. In each particular calculation, there are always two different Hamaker coefficients being calculated ($\mathcal{A}^{(0)}$ and $\mathcal{A}^{(2)}$). The $\mathcal{A}^{(0)}$ calculations have the trigonometric functions phase offset by 90°, which represents the orthogonal arrangement. When the trigonometric functions are brought into phase, there is an additional term $\mathcal{A}^{(2)}$ that represents the anisotropy arising from the orientation component. The largest amount of anisotropy will occur when the in-phase and 90° out-of-phase end points are drastically different. For the far-limit rod-rod $[9,3,m]$ system, the large values of $\Delta_{\parallel}$ (18.5 at $n=1$) give a huge boost when multiplied together in the aligned arrangement. When offset by 90°, the maximum values of $\Delta_{\parallel}$ are multiplied by $\Delta_{\perp}$ like terms, which are always less than a magnitude of 1 and thus limits the size of the overall contribution. Therefore, large differences between $\Delta_{\parallel}$ and $\Delta_{\perp}$ give insight as to the degree of anisotropy of the Hamaker coefficients.

When moving to the near-limit geometries addressed in this paper, the mismatch functions at a given frequency are always less than 1 because of their $\frac{\epsilon_L - \epsilon_m}{\epsilon_L + \epsilon_m}$ form. This limits the achievable anisotropy and overall Hamaker magnitude in ways described in the previous two sections. Furthermore, we no longer have $\Delta_{\parallel}$ for the aligned geometry, but rather γ. While γ is similar to $\Delta_{\parallel}$ in its $\frac{L-m}{m}$ form, its overall magnitude at each summation frequency n is smaller in size because the parallel and perpendicular directions are much closer to each other than that of the water medium (see Fig. 6), at least for all Matsubara frequencies above $n=2$. Lastly, the effect of γ on anisotropy is decreased further because it is found under a square-root sign. Still, despite all of these different dampening effects, anisotropy is still visible in the $[9,3,m]$ because

of the large mismatch in the axial and radial spectra at low frequencies. For the $[6,5,s]$, the values of γ are already very small and they get virtually wiped out within the $\sqrt{1+\gamma}$ term.

However, regardless of the smaller values of the Hamaker coefficient and of anisotropy in the near limit, we must remember the scale factor behaves as the far limit until the crossover point ℓ_0, which we have found to be at surface to surface separation distances approximately a CNT radii away. Therefore, if the different entities are indeed attracting each other up until the point of contact, then alignment can occur at all distances beyond this small crossover separation distance. In short, alignment considerations in the far limit should always be relevant when interacting with an optically anisotropic substrate or other optically anisotropic materials.

D. Practical matters

Much of the discussion thus far has been targeted toward understanding the nuts and bolts of the equations themselves. However, we would also like to address a few things that are of interest to the pragmatic experimentalist who may just want to use the equations or know how strong these energies are relative to thermal energy or other colloidal materials.

First, it is important not to forget that the Hamaker coefficient is not the only part of the entire vdW-Ld energy calculation. To get the final vdW-Ld energy, the Hamaker coefficient must be multiplied by the SWCNT length because almost all of the equations given have Hamaker coefficients that are per unit length. Thus, even a seemingly "small" Hamaker coefficient can result in an interaction energy much larger than the thermal energy simply because of length. For example, a 1-μm-long $[6,5,s]$ SWCNT at a distance of 2 nm from a gold substrate has a calculated vdW-Ld energy of approximately -221 kT at room temperature. A 100 nm rod would have a tenth of that, or approximately -21 kT of vdW-Ld energy interaction.

It is also this "per unit length" aspect that can make even very small values of the $\mathcal{A}^{(2)}$ or torque component of the Hamaker coefficient become very relevant with respect to total vdW-Ld energy considerations. For example, in Fig. 8 the Hamaker coefficient of the $[9,3,m]$ SWCNT is a 2.7 zJ greater when its axial direction aligns with that of the packed array anisotropic substrate. This yields an additional -4 kT of attractive vdW-Ld energy for a SWCNT length of 1 μm at a separation distance of 2 nm.

The next question of importance is whether or not one can glean the same amount of information using a component analysis as we did in our initial paper on the subject of anisotropic optical spectra of SWCNTs.[13] If one is uninterested in differentiating the energies between respective SWCNT chiralities and merely wants a ballpark figure, then one can certainly use the simple methods for approximation purposes. However, if one is interested in trying to design experiments where one tries to separate particular chiralities from one another, then it becomes imperative to use the full equations. Although the spectra will be exactly the same, the different formulations weight the mismatch in the neighboring spectrum in different ways, as can be seen by the previous sections describing the effects of $\Delta_\parallel$, $\Delta_\perp$, and γ.

Finally, it is useful to compare the magnitudes of SWCNT Hamaker coefficients in water to other materials commonly found in colloidal systems, such as beads and/or particles of polystyrene, Al_2O_3, graphite, and gold. Using the same index-matching water spectrum as the intervening medium and the semi-infinite biaxial plane-plane Lifshitz formulation (graphite is anisotropic and we need to account for both directions), we calculate values of 10, 60, 97, and 221 zJ for the polystyrene, Al_2O_3, graphite, and gold systems, respectively. The gold spectrum was obtained from experimental data in Palik,[26] the graphite spectra was obtained from our previously reported *ab initio* optical properties,[13] and the experimental Al_2O_3 and polystyrene spectra were obtained by vaccum ultraviolet and electron-energy-loss measurements found in the literature.[21,35] As we can see, the SWCNTs have Hamaker coefficients that are much more attractive than those of the polymer material but are not quite as strong as metals like gold. The overall values tend to be just as strong or stronger than those of graphite and titanium particles in solution.

VI. CONCLUSIONS

We have derived a consistent form of vdW-Ld interactions in the framework of the Lifshitz formulation for optically anisotropic cylinders and substrates. This formulation takes into account the optical and morphological anisotropies of SWCNTs and yields a quantitative estimate of the vdW-Ld interactions in terms of the appropriate Hamaker coefficients. Though the dependence of the interaction energy on the separation is, in general, complicated, we were able to derive two limiting cases, i.e., the far and near limits that allow for explicit analytical expressions for the interaction free energy. We have used these two explicit limiting forms to construct an interpolation formula valid for all intermediate separations and all orientations of the principal axes of the dielectric media involved. We were able to estimate that the crossover between the near and the far limit is at a surface-surface separation of approximately 1 SWCNT radius.

We have used these analytical developments to calculate the appropriate nonretarded Hamaker coefficients over the whole separation and orientation range of the interactions, for three conveniently chosen cases: a CNT interacting with an isotropic semi-infinite substrate, a CNT interacting with an anisotropic semi-infinite substrate, and a CNT interacting with another CNT. In the first case, the substrate was gold, and in the second, it was an ordered array of CNTs. In all three cases the medium was water. For all cases analyzed, the dielectric spectra are known and allow a straightforward computation of the separation as well as orientation dependence of the van der Waals interaction free energy. This dependence has been quantified via two Hamaker coefficients, one giving the magnitude of the orientation-independent part of the interaction and the other one accounting for the orientational part. In this way we were able to show the strong orientational dependence of the far-limit Hamaker coefficient for two metallic $[9,3,m]$ CNTs interacting with each other across a water medium. We have also shown similar strength

and orientation behaviors in the far-limit Hamaker calculations for a metallic $[9,3,m]$ over a substrate comprised of a hexagonal packed array of $[9,3,m]$ CNTs in water, predicting to drive an orientational ordering or torque upon approaching CNT from an orthogonal to a collinear configuration. We have also shown that, contrary to a $[9,3,m]$ CNT, the $[6,5,s]$ CNT has a much weaker directionally dependent Hamaker coefficient for both the rod-rod and rod-substrate systems in either limit. These results should guide future formulations that consider retardation, salt within the medium, and multilayer geometrical arrangements.[32–34]

The formulations are different from previous semi-infinite plane-plane interactions in that they introduce other components ($\Delta_\parallel$, $\Delta_\perp$, and γ as well as trigonometric functions) which alter the influence on how strongly the spectral mismatches influence the resulting Hamaker coefficient. Their importance lies in the calculation not only of orientation ef-

fects but also of the overall difference in magnitude between different SWCNT chiralities and a substrate. Knowing the difference of these magnitudes is useful for those interested in solution separation of SWCNTs based on the chirality-dependent vdW-Ld interaction energies.

[1] S. Iijima, Nature (London) **354**, 56 (1991).

[2] V. N. Popov, Mater. Sci. Eng., R. **43**, 61 (2004).

[3] C. T. White and J. W. Mintmire, J. Phys. Chem. B **109**, 52 (2005).

[4] I. Cabria, J. W. Mintmire, and C. T. White, Phys. Rev. B **67**, 121406(R) (2003).

[5] One important thing to note is that these labels only describe the electronic conduction properties along the axial direction of the SWCNT and are unrelated to the electronic conduction properties in the radial direction and the SWCNTs' optical properties in either direction.

[6] P. Lambin, C. R. Phys. **4**, 1009 (2003).

[7] W. Y. Ching, J. Am. Ceram. Soc. **71**, 3135 (1990).

[8] R. H. French, S. J. Glass, F. S. Ohuchi, Y. N. Xu, and W. Y. Ching, Phys. Rev. B **49**, 5133 (1994).

[9] W. Y. Ching, Y. N. Xu, and R. H. French, Phys. Rev. B **54**, 13546 (1996).

[10] Y. N. Xu, W. Y. Ching, and R. H. French, Phys. Rev. B **48**, 17695 (1993).

[11] Y. N. Xu and W. Y. Ching, Phys. Rev. B **51**, 17379 (1995).

[12] J. W. Mintmire and C. T. White, Synth. Met. **77**, 231 (1996).

[13] R. F. Rajter, R. H. French, W. Y. Ching, W. C. Carter, and Y. M. Chiang, J. Appl. Phys. **101**, 054303 (2007).

[14] Ge. G. Samsonidze, R. Saito, N. Kobayashi, A. Gruneis, J. Jiang, A. Jorio, S. G. Chou, G. Dresselhaus, and M. S. Dresselhaus, Appl. Phys. Lett. **85**, 5703 (2004).

[15] J. Israelachvili, *Intermolecular and Surface Forces*, 2nd ed. (Academic, New York, 1991).

[16] E. M. Lifshitz, Sov. Phys. JETP **2**, 73 (1956).

[17] V. A. Parsegian, *Van der Waals Forces* (Cambridge University Press, Cambridge, 2005).

[18] W. Y. Ching, M. Z. Huang, Y. N. Xu, W. G. Harter, and F. T. Chan, Phys. Rev. Lett. **67**, 2045 (1991).

[19] M. Hanfland, H. Beister, and K. Syassen, Phys. Rev. B **39**, 12598 (1989).

[20] D. Y. Smith, in *Handbook of Optical Constants of Solids*, edited by E. D. Palik (Academic, New York, 1985), Vol. I, p. 35.

[21] R. H. French, J. Am. Ceram. Soc. **83**, 2117 (2000).

[22] K. van Benthem, G. Tan, R. H. French, L. K. DeNoyer, R. Podgornik, and V. A. Parsegian, Phys. Rev. B **74**, 205110 (2006).

[23] See http://sourceforge. net/projects/geckoproj

[24] J. Chun, J. L. Li, R. Car, I. A. Aksay, and D. A. Saville, J. Phys. Chem. B **110**, 16624 (2006).

[25] The nonretarded case applies at small induced-dipole separations when $\omega d/c$ is small and no phase lag develops between the oscillations of the induced dipoles due to a finite speed of light, c.

[26] *Handbook of Optical Constants of Solids*, edited by E. D. Palik (Academic, New York, 1985), Vol. I; (Academic, New York, 1991), Vol. II; (Academic, New York, 1998), Vol. III.

[27] F. Wooten, *Optical Properties of Solids* (Academic, New York, 1972), p. 49.

[28] H. D. Ackler, R. H. French, and Y. M. Chiang, J. Colloid Interface Sci. **179**, 460 (1996).

[29] R. R. Dagastine, D. C. Prieve, and L. R. White, J. Colloid Interface Sci. **231**, 351 (2000).

[30] K. M. Knowles, J. Ceram. Proc. Res. **6**, 10 (2005).

[31] K. M. Knowles and S. Turan, Ultramicroscopy **83**, 245 (2000).

[32] B. W. Ninham and V. A. Parsegian, J. Chem. Phys. **52**, 4578 (1970).

[33] R. Podgornik and V. A. Parsegian, Phys. Rev. Lett. **80**, 1560 (1998).

[34] R. Podgornik, R. H. French, and V. A. Parsegian, J. Chem. Phys. **124**, 044709 (2006).

[35] R. H. French, K. I. Winey, M. K. Yang, and W. Qiu, Aust. J. Chem. **60**, 251 (2007).